EVLA Memo No. 223

SpaceX-VLA Alamo Pilot Testing

Chris De Pree, Urvashi Rau, Rob Selina, Brian Svoboda, Anthony Beasley

April 15, 2023

Abstract

In late 2021, NRAO began to consider how to help solve an ongoing issue with broadband internet access on the Alamo Navajo Reservation near the VLA site. By March 2022, in discussion with representatives from the Alamo tribe and SpaceX, NRAO developed a plan to help with the installation of ~60 Starlink User Terminals (UTs) at family residences. This action was taken to help provide families on the reservation with decentralized broadband internet access for education. An equally important goal of this installation of Starlink UTs at a location that previously had no broadband internet access, was to evaluate the impact on normal VLA operations. For the past year, NRAO has been performing at first bi-weekly and then monthly monitoring of the frequencies utilized by SpaceX (and other satellite operators) for RFI in the uplink (14.0-14.5 GHz) and downlink (10.7-12.7 GHz) bands. In this report, we summarize the preliminary analysis of selected datasets from the first year of monitoring, and describe the plan for ongoing monitoring and a full analysis of these data.

1 INTRODUCTION

Broadband access is a critical issue for rural populations. The Very Large Array is located in a county with low levels of fixed broadband access, and NRAO understands the importance of this issue for populations living near its telescopes. In early 2022, NRAO began to develop a plan to help address the ongoing issue of broadband internet access on the Alamo Navajo Reservation near the VLA site. This issue was highlighted by the need for broadband access for education during the peak of the COVID-19 pandemic.

By March 2022, NRAO in discussion with representatives from the Alamo Navajo Reservation[1] and SpaceX decided to facilitate the installation of ~60 Starlink User Terminals (UTs) at family residences located on the reservation. This action was taken to help provide families with decentralized broadband internet access for education. Another goal of this project was to pilot the installation of Starlink UTs at a location near the VLA, and evaluate the impact on normal VLA operations. The full technical specifications of the Starlink system and the UTs installed are described in EVLA Memo 222 "Coordinated Starlink User Terminal Testing Near the VLA".[1]

UTs were installed at the Alamo Reservation starting on March 18, 2022. The last installation took place on June 27, 2022. The table in Appendix A shows the GPS locations of each of the 59 installed UTs, and the date when each was installed, along with a column recording observations made with the VLA in various configurations to monitor the RFI environment as the UTs were installed. Two observations were made before any UTs were installed to establish a baseline RFI environment. Successive VLA observations were made after the installation of a total of 15, 33, 37, 50 and 59 UTs. Since the completion of UT installations, in June 2022, continuing VLA observations have been made approximately once per month.

---

[1] The Alamo Navajo Reservation is located approximately 20 km to the NE of the end of the North arm of the VLA in its largest (A) configuration, and ~36 km from the VLA center.

The first observation in the VLA D-configuration was made 7/28/2022 after all 59 UTs were installed. The most recent observations (at the time of this memo) were made on April 16, 2023 (B configuration). Interferometric attenuation theory (Thompson [2]; Perley [3]) and the results of the 2021 SpaceX-VLA testing (EVLA Memo 222) indicated that RFI presents the highest possible impact on observations when the VLA is in its smallest configuration with the largest proportion of short baselines.

In Section 2, we describe the background and simple estimates of the impact of space-based RFI on interferometric imaging. In Section 3, we describe the experimental setup, and in Section 4, we present early results from the first year of data.

2 BACKGROUND AND ESTIMATES

We will modify the methodology used by Perley [3] to estimate the attenuation of a fixed interferer by an imaging interferometer using earth rotation synthesis. We will use the VLA in D-configuration as a limiting case, given its short baselines.

Perley computes the interferometer attenuation factor for a fixed RFI source to be:

$$R(t) \sim \frac{1}{\sqrt{\pi} N_a} \sqrt{\frac{\lambda}{\omega_e t B_m \cos(\delta)}}$$

Where the distance travelled in the image by the geostationary interferer is $\omega_e t\cos(\delta)$. For a LEO satellite, which moves much faster than the phase center across the sky, we can approximate the distance traveled as $\omega_{sat} t$. We can then approximate the interferometric attenuation factor due to LEO satellite motion to be:

$$R(t) \sim \frac{1}{\sqrt{\pi} N_a} \sqrt{\frac{\lambda}{\omega_{sat} t B_m}}$$

For the VLA in D-Configuration, the key parameters are N_a=27 and B_m= 250m. For λ = 2.8cm, $\omega_{sat} = 0.25°/sec,$ and t = 1, 10, 100, and 1000 we can compute that R is roughly 25dB, 30dB, 35dB and 40dB, respectively. This estimate could even be conservative for longer timescales, as the interferer will be spread over many (*u,v*) cells, and the effect on imaging could therefor decline as $1/M$ rather than $1/\sqrt{M}$ [3].

Including this attenuation factor when assessing the power spectral density levels in EVLA Memo 222 suggests that (1) the VLA should be capable of imaging (at least at moderate dynamic range) over the LEO transmit range when satellite sidelobes are received through antenna sidelobes, and (2) the interferometric attenuation may be sufficient to image even in the case where the satellite is illuminating the VLA site, but is received through an antenna sidelobe, for all but the shortest projected baselines. These results should be considered 1st order approximations, and the true impact on imaging (dynamic range limits and noise floor) should be assessed through further testing and/or simulations.

3 VLA EXPERIMENTAL SETUP

All VLA monitoring observations in this experiment are carried out at the downlink frequencies (10.7 - 12.7 GHz) in X band and Ku band and at the uplink frequencies (14.0 - 14.5 GHz) in the Ku band using the VLA. The primary flux density calibrators are 3C48 and 3C286, depending on the time of year of the observations. For each observation, we have made images of an offset field. To avoid imaging artifacts from bright astronomical sources, we have selected target fields offset from 3C48 by approximately ten degrees, centered at J2000 (α, δ) = (0h 39m 35.811s, 34d 32′ 57.02″), and offset from 3C286 centered at J2000 (α, δ) = (12h 39m 36.8672s, 30d 57′ 48.772″), We use 3C48 or 3C286 for flux and bandpass calibration as well as for gain calibration for the offset field. Total on-source integration times for the offset target field are approximately ten minutes in both X and Ku Bands. We configured the VLA WIDAR correlator using the 8-bit samplers and a 1sec visibility integration (dump) time.

X-band observations: The X Band tuning observed two 1 GHz-wide basebands centered on 10.7 GHz and 11.7 GHz. Each baseband contains eight 128 MHz dual-polarization sub-bands containing 128-1 MHz channels for a total bandwidth of 2.048 GHz. This frequency range covers Starlink downlink channels 1 through 6, although channel 6 is observed with degraded sensitivity due to observing into the filter roll-off at the receiver band edge.

Ku-band observations: The Ku Band tuning observed two 1 GHz-wide basebands centered at 12.33 GHz and 14.25 GHz to measure downlink channels 6 through 8 and all 8 uplink channels. The first baseband is equivalent to the X Band setup of eight 128 MHz adjacent sub-bands with 128-1 MHz channels in dual-polarization mode. For finer frequency resolution on uplink channels, the second baseband from 13.75-14.75 GHz (fully covering the User Terminal uplink channels in the 14.0-14.5 GHz range) uses eight 128 MHz adjacent sub-bands with 256 500 kHz dual-polarization channels.

Note that the uplink frequencies are covered in a single band (Ku), but the downlink frequencies are covered in two bands (X and Ku). This leads to some needed fine-tuning in pipeline data reduction where the goal is to separate the uplink and downlink bands (the pipeline default is to combine all SPWs in a single band together). Current scripts accomplish this separation by imaging at the end of the pipeline script with a specific *tclean* command (sample inputs in Appendix B). Individual observations are part of queued observing, so we have not been able to keep the observations to the same time of day (being at similar LST). Since Internet usage is expected to vary by time of day, this should be kept in mind when inferring trends. Also we are unsure if Internet usage has gone up or down even with the same number of terminals deployed (since June 2022). We have asked SpaceX for usage information as it may help with ongoing interpretation of these data.

4 YEAR 1 MONITORING RESULTS

As of the publication of this memo, monitoring observations have been carried out in all four configurations of the VLA. The conclusions drawn from this memo represent the measured impact of the operation of 59 UTs in the proximity of the VLA north arm through one full cycle of configurations. As was first discovered in the initial Starlink tests performed in late 2021 (EVLA Memo 222), the downlink transmissions appear to be much more easily detected by the VLA than uplink transmissions given the RFI attenuation afforded by topography.

NRAO Spectrum Management and NM Operations will continue to perform monitoring runs, and update the results presented in this memo annually. The criteria used in judging the image fields will be continued in future observations and analysis, namely, the rms noise in the offset field for each observation. We expect the RFI measured in 2023 (with only about 4000 satellites in orbit in the SpaceX Starlink constellation) to be lower than it will be in coming years as the full constellation Starlink is deployed.

4.1 DATA PROCESSING

All datasets are pipeline processed using the CASA-VLA data reduction pipeline. The standard script used is given in Appendix B. Data presented in this memo sample the period of UT installation, and all four configurations of the VLA, and include observations made on the following dates (VLA configuration in parentheses): 3-14-22 (A), 6-6-22 (A), 9-9-22 (D), 12-2-22 (C), 01-22-23 (B).

Additional datasets from the past year have also been pipeline processed, but are not presented in this memo. Dates for all VLA observations related to this monitoring are provided in Appendix A.

This memo provides a first look at this monitoring project, and we will continue the work during summer 2023 with a summer student fully reducing all datasets in hand to complete the analysis of the existing observations.

4.2 UPLINK RESULTS

As was found with the first round of UT testing performed near the VLA in September 2021 (EVLA Memo 222), the uplink channels show little evidence of uplink signals in the 14.0-14.5 GHz range (sample of the calibrated visibilities colored by spectral window in Fig. 1 are from the 12-02-2022 observations, made with VLA in the A-configuration).

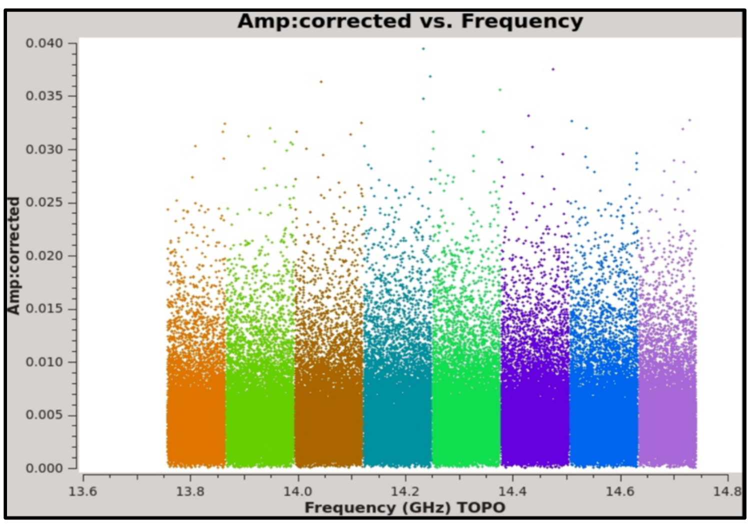

Fig. 1 Calibrated uplink passband from Ku-band data (12-02-2022, C configuration). For finer frequency resolution on uplink channels, the baseband from 13.75-14.75 GHz (fully covering the User Terminal uplink channels in the 14.0-14.5 GHz range) uses eight 128 MHz adjacent sub-bands with 256 500 kHz dual-polarization channels.

For comparison, the uplink channels shown in Fig. 2 are from the 07-28-2022 observations (D configuration). We expect to see more RFI in configurations with more short baselines (Perley 2002). While there is some narrowband RFI apparent (~14.44 GHz), the RFI signal does not have the characteristic width of a SpaceX UT uplink signal (e.g. ~60 MHz bandwidth).

Note that with the exception of this narrowband RFI signal, the visibility amplitudes in the uplink channels between these two runs are similar. Table 1 indicates that for the representative observations made over the past year, there is no systematic increase in rms noise in Ku band (or specific uplink SPW) images generated by standard pipeline calibrations, either during the installation, or once all ~60 UTs were installed.

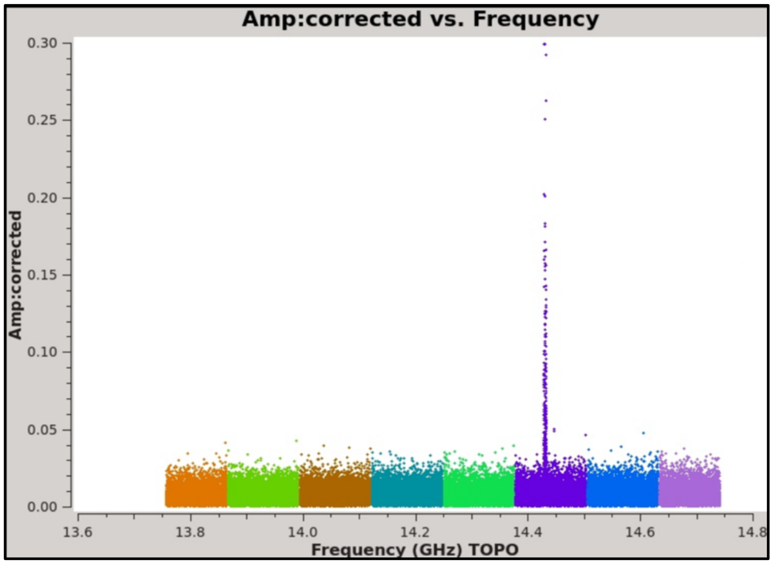

Fig. 2. Narrow band RFI apparent in the uplink frequency range for UT to satellite (14.0-14.5 GHz). These data are from 07-28-2022 observations (D configuration)

4.3 DOWNLINK RESULTS

The results of the first coordinated SpaceX/VLA tests (EVLA Memo 222) indicated that the downlink signals were more likely to be detected than the uplink signals. Since the current monitoring tests are not coordinated with SpaceX, it is impossible to correlate a specific RFI signal with a transmission from a SpaceX satellite (as we were able to do in the coordinated testing described in EVLA Memo 222). However, since the UTs are installed and operational within the Alamo reservation, we know that SpaceX downlink beams are regularly illuminating the service cell containing the reservation. From the processed data presented in this Memo (see Table 1), we see no evidence of increasing rms noise in the offset faint field image as a function of time in X-band (generally) or in the downlink SPWs (which include all of X and part of Ku band).

Table 1 shows the rms noise value in the faint source field for observations made with the VLA on the dates indicated. The rms values are mostly taken from the pipeline processed images (as indicated in the h_makeimages(cont) output). In a few cases (as noted), images have been generated for the offset field using only uplink (SPW 2~9) and only downlink (SPW 10~33) spectral windows. In the table, these rms values are indicated in parentheses. A sample faint source field is shown in Fig. 3.

The default pipeline calibration groups SPWs together by band (e.g. uplink → Ku band, downlink → X band). When the SPWs are more properly separated by process (uplink or downlink), there is less bandwidth in the uplink observation (such that the rms noise increases in the image) and more bandwidth in the downlink observation (such that the rms noise decreases in the image). In the final analysis of these data, all observations will have uplink and downlink separated in this same way. However, even with the data as currently reduced, it is apparent that there does not appear to be any change in image rms as the UTs were installed (compare the rms noise figure in the 3-14-22 and 6-6-22 runs that bracket the installation of most of the UTs), or over time in the past year.

Date (Configuration)	X Band (Downlink Only) *rms (microJy/beam)*	Ku Band (Uplink Only) *rms (microJy/beam)*	UTs Installed
3-14-22 (A)	11	10 (15)	0
6-6-22 (A)	11	9.6	50
9-9-22 (D)	19	14	59
12-2-22 (C)	11 (8.7)	10.5 (13.7)	59
01-22-23 (B)	11 (8.5)	9.8	59

Table 1 The rms noise as measured in the Ku-band and X-band spectral windows in pipeline data reduction for the selected representative observations. The two different A-configuration observations span the installation of most of the UTs during the spring of 2022, and the remaining observations provide a representative observation in each of the other VLA configurations. Values in parentheses show the noise in the specific uplink and downlink SPWs only.

Below is a sample image from the faint source field from the 2022-12-02 (C configuration) observations. This image includes all downlink (10.7-12.7 GHz) spectral windows (CH 1-6 from X band and CH 6-8 from Ku-band). Beam is indicated in the lower left of the figure. The three visible sources range in peak flux density from 0.17 to 1.5 mJy/beam.

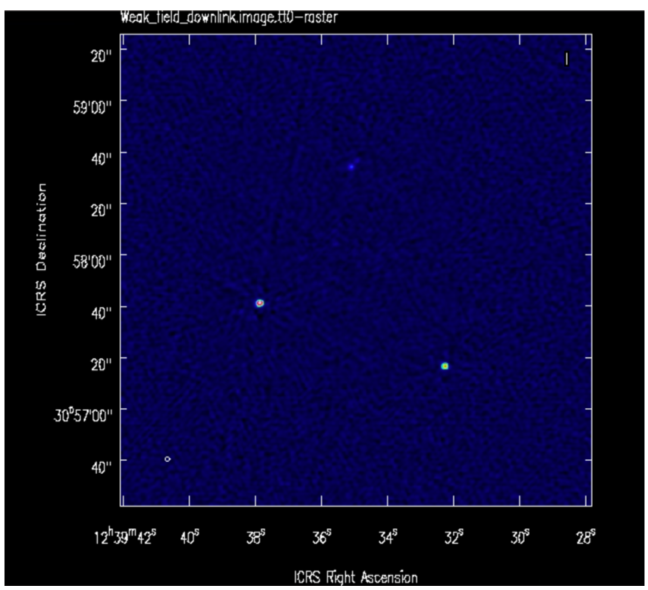

Fig.3 "Faint source field" image from 12-02-2022 (C configuration) made with all downlink spectral windows (CH 1-6 from X band and CH 6-8 from Ku-band). The rms noise in this image is ~8.7 microJy/beam.

In one example of the difference in detected RFI between similar observations, Figures 4 and 5 show the initial test bandpass calibration of the X and Ku-band data before flagging commands were applied by the pipeline. These two observations, made with the same antenna configuration (C) indicate that many other variables (e.g. time of day) surely impact the detected RFI. We note that the 10-06-22 and 12-02-22 observations are separated by about 12 hours, with the 12-02-22 observations made at about 4 PM and the 10-06-22 observations made at about 4 AM.

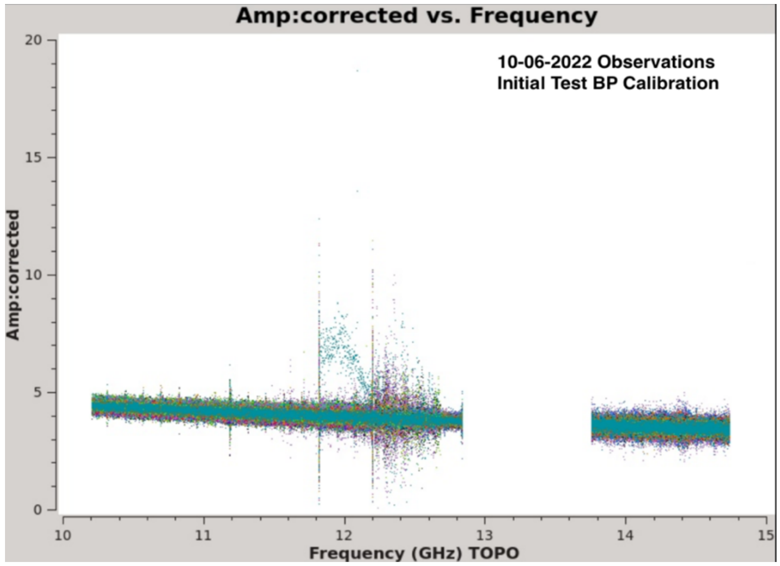

Fig. 4 Initial Test bandpass calibration of C-configuration observations on 10-06-2022. Observations were made at about 4 AM local time.

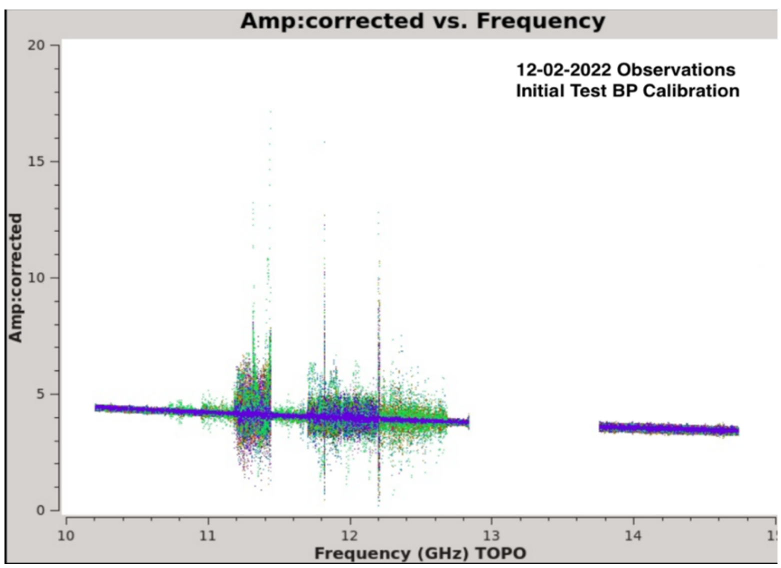

Fig. 5 Initial Test bandpass calibration of C-configuration observations on 12-02-2022. Observations were made at about 4 PM local time.

4.3.1 Impact of Baseline Length

As expected, in downlink channels, the detected RFI (before flagging) is worse in short baselines as seen in Figures 6 and 7. Figure 6 shows the calibrated amplitudes in the long baselines while Figure 7 shows RFI in the short baselines. There is persistent RFI (likely the result of geostationary satellites) at the high end of this 10.7-12.75 GHz frequency range.

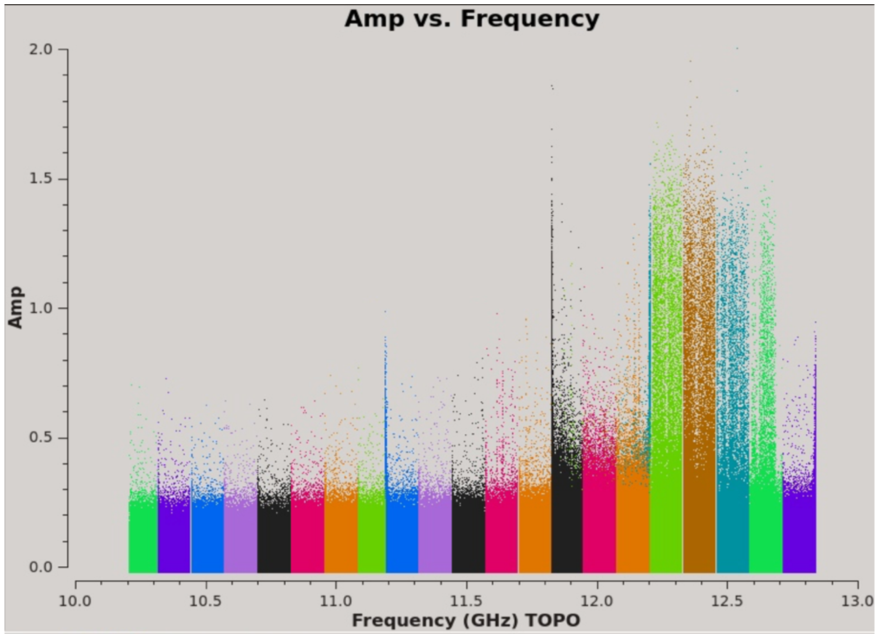

Fig. 6 Observations from 12-27-22 (C configuration) covering the SpaceX downlink channels (11.2-12.75 GHz). This plot of corrected amplitude versus uv-distance shows long baselines only (uv distance>1200). Note that in these data, RFI is mostly apparent at frequencies >12.2 GHz.

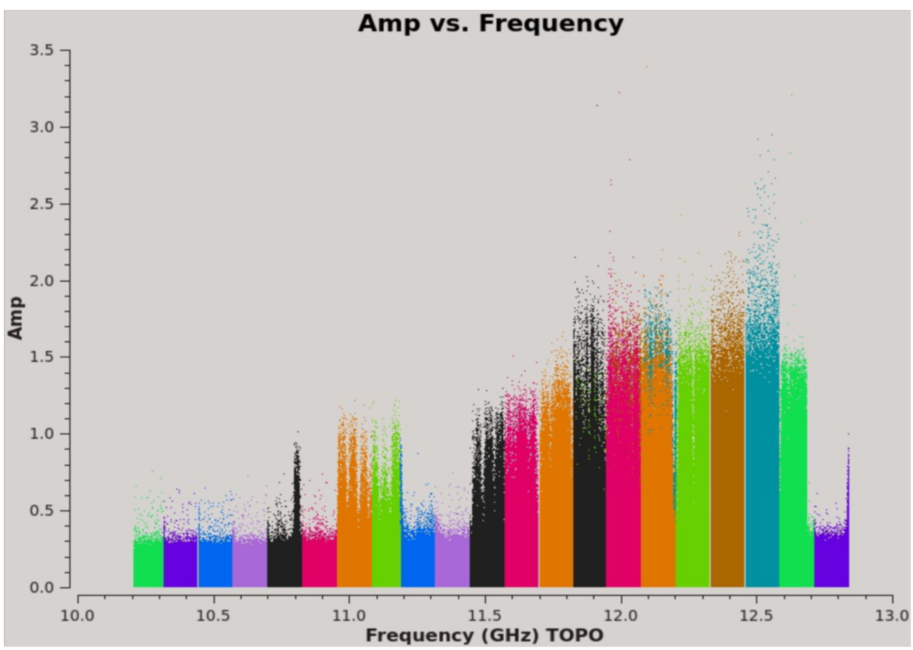

Fig. 7 Observations from 12-27-22 (C configuration) covering the SpaceX downlink channels (11.2-12.75 GHz). This plot of corrected amplitude versus uv-distance shows short baselines only (uv distance<1200). Note that in these data, RFI is apparent at frequencies from 10.7 GHz - 12.7 GHz. The emission detected in the 10.95-11.2 GHz frequency range is associated with SpaceX downlink Channel 2, but SpaceX satellites are not currently outfitted with transmitters in this frequency range. These transmissions are likely from another space-borne transmitter.

As of late January 2023, when the VLA moved into the B configuration, we had acquired datasets from the full cycle of VLA configurations (A, B, C, D). We will continue to monitor and process these datasets as they are taken. Because the downlink frequencies have other users besides Starlink, it may be difficult to attribute any changes in the RFI environment to one LEO constellation alone.

5 CONCLUSIONS

Early indications from the data are that both uplinks and downlinks from ~60 UTs located at the Alamo Navajo Reservation are having minimal impacts on the normal operations of the VLA. Imaging performance in X-band and Ku-band appears to be resilient in the presence of this operating satellite service, at least with the current number of satellites and users. Note that the actual usage load at the times of the test observations is currently not known and this information would be required prior to making any predictive conclusions. Monitoring will continue at a regular cadence through the configuration cycle, approximately once per month. These ongoing experiments can provide testbed data for modeling and estimates of RFI impacts on the ngVLA [4].

6 REFERENCES

[1] De Pree, C. et al. "Coordinated Starlink User Terminal Testing Near the Very Large Array" EVLA Memo #222, April 2023.

[2] Thompson, A. R. "The Response of a Radio-Astronomy Synthesis Array to Interfering Signals" IEEE Transactions on Antennas and Propagation, Vol. AP-30, No. 3, May 1982, pp. 450 - 456.

[3] Perley, R. "Attenuation of Radio Frequency Interference by Interferometric Fringe Rotation" EVLA Memo #49, November 2002.

[4] Selina et al. "Updated RFI Impact Estimates & Influence on the System Design", ngVLA Memo #109, April 2023

7 ACKNOWLEDGEMENTS

The authors would like to acknowledge the instrumental work of James Robnett and the Alamo Navajo Reservation in setting up the User Terminals that enabled these tests and the ongoing support of SpaceX. The authors additionally acknowledge John Tobin for help with CASA data reduction scripts.

APPENDIX A – SPACEX UT INSTALLATION AND VLA OBSERVATION SCHEDULE

UT Number	Alamo UT Locations		Installation	VLA Run	UTs Installed	VLA
	Lat	Long	Date	*Date*	*Total*	Configuration
				3/4/22, 3/14/22	0	A
21	34°24'32.88"N	107°29'33.49"W	03/18/22			
2	34°29'4.78"N	107°31'18.58"W	03/23/22			
16	34°24'28.2"N	107°30'25.6"W	03/23/22			
25	34°24'26.9"N	107°28'55.1"W	03/23/22			
3	34°28'27.8"N	107°31'16.0"W	03/25/22			
7	34°26'21.27"N	107°31'5.82"W	03/25/22			
8	34°26'16.2"N	107°30'55.5"W	03/25/22			
10	34°25'25.85"N	107°30'15.32"W	03/25/22			
29	34°23'30.4"N	107°29'46.6"W	03/25/22			
15	34°24'26.1"N	107°30'29.9"W	03/28/22			
26	34°24'3.65"N	107°29'19.42"W	03/28/22			
30	34°23'22.5"N	107°29'47.0"W	03/28/22			
38	34°22'40.4"N	107°28'25.2"W	03/28/22			
40	34°22'52.7"N	107°28'23.2"W	03/28/22			
44	34°23'11.2"N	107°28'11.0"W	03/28/22			
				3/28, 3/29	15	A
39	34°22'48.3"N	107°28'26.0"W	04/01/22			
41	34°22'56.8"N	107°28'29.3"W	04/01/22			
42	34°23'14.8"N	107°28'33.3"W	04/01/22			
50	34°22'14.6"N	107°26'15.9"W	04/01/22			
51	34°21'51.0"N	107°25'14.5"W	04/01/22			
52	34°21'53.7"N	107°24'45.2"W	04/01/22			
17	34°23'52.9"N	107°31'10.4"W	04/04/22			
20	34°23'43.6"N	107°31'46.5"W	04/04/22			

22	34°24'20.8"N	107°29'32.8"W	04/04/22			
32	34°22'18.9"N	107°29'54.3"W	04/04/22			
35	34°20'41.3"N	107°29'52.1"W	04/04/22			
36	34°20'36.8"N	107°29'51.3"W	04/04/22			
11	34°24'50.0"N	107°30'02.5"W	04/08/22			
47	34°22'22.7"N	107°26'49.2"W	04/08/22			
54	34°20'19.0"N	107°26'31.8"W	04/08/22			
56	34°21'05.0"N	107°26'28.7"W	04/08/22			
57	34°21'03.3"N	107°26'24.9"W	04/08/22			
59	34°21'17.0"N	107°26'22.2"W	04/08/22			
				4/9, 4/16, 4/22, 4/29, 5/12	33	A
1	34°29'40.81"N	107°31'13.15"W	05/23/22			
4	34°28'1.15"N	107°31'34.70"W	05/23/22			
6	34°26'27.92"N	107°30'55.26"W	05/23/22			
18	34°23'52.1"N	107°31'30.0"W	05/23/22			
				5/26	37	A
9	34°25'50.87"N	107°30'34.60"W	05/31/22			
14			05/31/22			
27	34°23'57.37"N	107°29'28.38"W	05/31/22			
28	34°23'39.8"N	107°29'50.0"W	05/31/22			
45	34°23'25.0"N	107°28'37.4"W	05/31/22			
5	34°27'30.94"N	107°31'24.72"W	06/03/22			
13			06/03/22			
19	34°23'45.3"N	107°31'27.5"W	06/03/22			
31	34°23'9.14"N	107°29'55.89"W	06/03/22			
43	34°23'16.4"N	107°28'20.6"W	06/03/22			
46	34°22'53.5"N	107°27'08.6"W	06/06/22			
48	34°22'19.7"N	107°26'27.1"W	06/06/22			
55	34°20'47.3"N	107°26'24.7"W	06/06/22			
				6/6	50	A

12	34°25'21.62"N	107°30'48.27"W	06/09/22			
33	34°21'23.8"N	107°29'51.7"W	06/09/22			
34	34°21'29.01"N	107°29'38.55"W	06/09/22			
49	34°22'17.7"N	107°26'29.4"W	06/09/22			
23	34°24'24.36"N	107°29'11.23"W	06/15/22			
24	34°24'20.74"N	107°29'15.29"W	06/15/22			
37	34°20'52.0"N	107°29'12.4"W	06/15/22			
53	34°19'41.2"N	107°26'42.4"W	06/15/22			
58	34°20'58.8"N	107°26'24.0"W	06/27/22			
				7/9, 7/28, 9/9, 10/6, 11/3, 12/2, 12/27, 1/22, 2-xx, 3-22	59	7/9 (move), 7/28(D), 9/9(D), 10/6 (C), 11/3 (C), 12/2 (C), 12/27 (C), 1/22/23 (C), 1/22 (B), 2-xx (B), 3-22 (B)

APPENDIX B – CASA PIPELINE SCRIPT

Below is the CASA pipeline script used to process the 12-02-2022 data. This same script has been used for the datasets presented in this memo.

```
# This CASA pipescript is meant for use with CASA 6.4.1 and pipeline 2022.2.0.64
context = h_init()
context.set_state('ProjectSummary', 'observatory', 'Karl G. Jansky Very Large Array')
context.set_state('ProjectSummary', 'telescope', 'EVLA')
try:
 hifv_importdata(vis=['TRFI0004.sb41206290.eb43036465.59915.47726306713'], \
  createmms='automatic', asis='Receiver CalAtmosphere', ocorr_mode='co', \
  nocopy=False, overwrite=False)
 # Hanning smoothing is turned off in the following step.
 # In the case of extreme RFI or very bright masers, Hanning smoothing
 # may still be required.
 #hifv_hanning(pipelinemode="automatic")
 hifv_flagdata(fracspw=0.01, \
  intents='*POINTING*,*FOCUS*,*ATMOSPHERE*,*SIDEBAND_RATIO*, *UNKNOWN*, \
  *SYSTEM_CONFIGURATION*, *UNSPECIFIED#UNSPECIFIED*', hm_tbuff='1.5int')
 hifv_vlasetjy(pipelinemode="automatic")
 hifv_priorcals(pipelinemode="automatic")
 hifv_syspower(pipelinemode="automatic")
 hifv_testBPdcals(pipelinemode="automatic")
 hifv_checkflag(checkflagmode='bpd-vla')
 hifv_semiFinalBPdcals(pipelinemode="automatic")
 hifv_checkflag(checkflagmode='allcals-vla')
 hifv_solint(pipelinemode="automatic")
 hifv_fluxboot(pipelinemode="automatic")
 hifv_finalcals(pipelinemode="automatic")
 hifv_applycals(pipelinemode="automatic")
 # Keep the following three steps in the script if cont.dat exists.
 # Otherwise we recommend to comment out the next task.
 hifv_checkflag(checkflagmode='target-vla')
 hifv_statwt(pipelinemode="automatic")
 hifv_plotsummary(pipelinemode="automatic")
 hif_makeimlist(intent='PHASE,BANDPASS',specmode='cont')
 hif_makeimages(hm_masking='centralregion')
 #Science target imaging pipeline commands
 hif_mstransform(pipelinemode="automatic")
# hif_checkproductsize(maximsize=16384)
# hif_makeimlist(specmode='cont')
# hif_makeimages(hm_cyclefactor=3.0)
# hifv_pbcor(pipelinemode="automatic")
# Make sure VIS is correct
 tclean(vis=['TRFI0004.sb41206290.eb43036465.59915.47726306713_targets.ms'],
       field='J1239+3057_wea',
       spw='2~9',#Uplink only
       uvrange='>6.2klambda',
       antenna=['0,1,2,3,4,5,6,7,8,9,10,11,12,13,14,15,16,17,18,19,20,21,22,23,24,25,26,27&'],
       scan=['7,9,14,16'], intent='OBSERVE_TARGET#UNSPECIFIED',
       datacolumn='data',
       imagename='Weak_field_uplink',
       imsize=[2160, 2160], cell=['0.34arcsec'],
       phasecenter='ICRS 12:39:36.8672 +030.57.48.772',
       stokes='I', specmode='mfs', nchan=-1, outframe='LSRK',
       perchanweightdensity=False, gridder='standard', mosweight=False,
       usepointing=False, pblimit=-0.1, deconvolver='mtmfs', nterms=2,
       restoration=True, restoringbeam='common', pbcor=True, weighting='briggs',
       robust=0.5, npixels=0, niter=799999, threshold='', nsigma=4.0,
       cyclefactor=3.0, interactive=0, usemask='auto-multithresh',
       sidelobethreshold=2.0, minbeamfrac=0.3, dogrowprune=True, restart=False,
       savemodel='none', calcres=True, calcpsf=True, parallel=False)
 tclean(vis=['TRFI0004.sb41206290.eb43036465.59915.47726306713_targets.ms'],
       field='J1239+3057_wea',
       spw='10~33',#Downlink only
       uvrange='>6.2klambda',
```

```
       antenna=['0,1,2,3,4,5,6,7,8,9,10,11,12,13,14,15,16,17,18,19,20,21,22,23,24,25,26,27&'],
       scan=['7,9,14,16'], intent='OBSERVE_TARGET#UNSPECIFIED',
       datacolumn='data',
       imagename='Weak_field_downlink',
       imsize=[2160, 2160], cell=['0.34arcsec'],
       phasecenter='ICRS 12:39:36.8672 +030.57.48.772',
       stokes='I', specmode='mfs', nchan=-1, outframe='LSRK',
       perchanweightdensity=False, gridder='standard', mosweight=False,
       usepointing=False, pblimit=-0.1, deconvolver='mtmfs', nterms=2,
       restoration=True, restoringbeam='common', pbcor=True, weighting='briggs',
       robust=0.5, npixels=0, niter=799999, threshold='', nsigma=4.0,
       cyclefactor=3.0, interactive=0, usemask='auto-multithresh',
       sidelobethreshold=2.0, minbeamfrac=0.3, dogrowprune=True, restart=False,
       savemodel='none', calcres=True, calcpsf=True, parallel=False)
 #hifv_exportdata(pipelinemode="automatic")
finally:
 h_save()
```